Okhotsk Sea and Polar Oceans Research 3 (2019) 13-19


Article

# Turning features of an icebreaker during ramming operations: a case study

Yuto TAKAHASHI[1], Hajime YAMAGUCHI[1], Shuki USHIO[2],
Yutaka YAMAUCHI[3] and Shigeya MIZUNO[3]

[1] *Graduate School of Frontier Sciences, The University of Tokyo, Kashiwa, Japan*
[2] *Meteorology and Glaciology Group, National Institute of Polar Research, Tachikawa, Japan*
[3] *Technical Research Center, Japan Marine United Corporation, Tsu, Japan*

(Received September 30, 2018; Revised manuscript accepted December 25, 2018)

**Abstract**

Syowa Station, Japan's main Antarctic research base, is located in Lützow–Holm Bay (LHB) This bay is often covered with very thick multiyear landfast ice. The Japanese Antarctic research icebreaker *Shirase II* conducts "ramming" icebreaking operations comprising repeating backing and ramming, sometimes thousands of times, in one cruise. In this study, we analyzed data for turning in ice while ramming, which is a rare occurrence. The turning angle per ramming procedure and the turning radius are correlated with the ramming penetration distance. Thus, the required time and ice area width for one turn can be estimated from the data of the first several ramming trials. In addition, shortening the approach run length decreases the time required per ramming procedure and the turning trajectory and increases the required number of ramming procedures. To balance these effects, we attempted to reduce the total required time by controlling the approach run length. It was concluded that the best operation to reduce the turning time is to use an approach run length that is sufficient to achieve high impact velocity, unless the brash ice in the broken channel significantly prevents the ship's astern movement.

**Key words:** icebreaker, ramming, turning, maneuverability, navigation support

## 1. Introduction

Syowa Station, Japan's main Antarctic research base, is located in Lützow–Holm Bay (LHB). This bay is often covered with very thick multiyear landfast ice. While icebreakers can usually navigate with continuous icebreaking, the ramming operations (i.e., backing and ramming) are required in areas where the ice thickness exceeds a certain level. In this operation, an icebreaker repeats the following procedure:

1. Move astern for an approach run
2. Accelerate using a channel (made by the previous ramming operation) and impact on ice at high speed
3. Penetrate using kinetic energy and propulsion thrust

This procedure requires significant time and fuel. In LHB, the Japanese Antarctic research icebreaker *Shirase II* (hereafter called *Shirase*) sometimes conducts thousands of ramming operations in one cruise.

During navigation under very heavy ice conditions, icebreakers sometimes need to turn during ramming operations. *Shirase* has made 180° turns during ramming operations in both the 2012/2013 and 2017/2018 cruises. Turning by 180° during ramming operations can require half a day or more, so its efficient execution is important.

Many studies (e.g., Daley and Riska, 1990) have investigated straightforward ramming performance. By contrast, only some studies (e.g., Nozawa, 2006) have investigated turning performance with continuous icebreaking, and little is known about turning ramming performance because this operation occurs rarely.

Owing to the low frequency of turning ramming operations, valuable data can be obtained from multiple turns with ramming by the same icebreaker. In this study, we investigate the turning of *Shirase* to determine principles for conducting more efficient turning and to provide information for navigation planning.

## 2. Method

Table 1 lists the main dimensions of *Shirase* (for other specifications, refer to Yamauchi and Mizuno, 2009). *Shirase*'s navigation data is recorded using a ship-monitoring system (SMS) that records basic navigation information including GPS location (accuracy: < 10 m), ship motion, steering angle, and engine power (Yamauchi et al., 2011). Navigation data of four turns from the last nine years are extracted analysis (Table 2). The ice thickness values ($h$) observed during the turns are shown in the table only as guides; they are roughly estimated by image analysis of photos taken with a compact digital camera (2012/2013) and by unaided visual observation (2017/2018). Slash-delimited numbers indicate

observed samples. Image analysis is conducted based on the same principle as the video method conducted since 1988 (Shimoda et al., 1997). However, it is considered less accurate than the video method because the compact camera was not fixed, which may have caused large variations in observed values. Although the ice thickness may vary during a turn, we did not consider this in this study because of the lack of high-precision data with high sampling density.

The inner part of LHB contains "landfast level ice" (Turns 1–3) of high and stable thickness. Furthermore, "Hummock ice" of variable thickness develops on the ice edge.

Table 1. Main dimensions of *Shirase* (Yamauchi and Mizuno, 2009)

| | |
|---|---|
| Overall length | 138.0 m |
| Length of water line | 126.0 m |
| Maximum breadth | 28.0 m |
| Depth | 15.9 m |

Table 2. General descriptions of analyzed turns

| | Season | Ice feature | Ice thickness (m) |
|---|---|---|---|
| Turn 1 | January, 2013 | Landfast level ice | 2.6 / 4.0 |
| Turn 2 | February, 2013 | Landfast level ice | 4.2 / 4.4 / 5.2 |
| Turn 3 | January, 2018 | Landfast level ice | 1.7 / 2.1 |
| Turn 4 | February, 2018 | Hummock ice near ice edge | 2.1 / 2.2 |

The navigation data is analyzed through the three steps described below.

**1) Ramming section extraction and characteristic parameter calculation for each ramming procedure**

In this study, one ramming procedure is defined from starting astern movement to stopping the ship body after penetrating the ice. Fig. 1 shows an example of a ramming procedure extracted from SMS data. The shaft speed and rudder angle are the average of two values. A ramming procedure is decomposed into three phases:

**A) Astern**

This phase is defined from stopping the previous ramming procedure to starting the next approach run, including a few minutes for reversing the engine rotation. The ship speed is controlled carefully to avoid collisions with the ice, typically by changing the shaft speed at a rate <120 rpm to maintain a velocity of <1.5 m/s. The rudder is kept neutral during astern movement to avoid damage, and the traveling direction is controlled by changing the balance of the left–right thruster output. For typical ramming navigation of *Shirase*, the astern distance (identical to the approach run length discussed below) is ideally 300 m. The actual astern distance must sometimes be shorter mainly because brash ice fills the channel and reduces the efficiency of astern movement. The astern distance can also be reduced intentionally when ramming partially weak or cracked ice. Such operations are often used with hummock ice.

**B) Approach run**

After the astern movement phase, the ship accelerates with high engine power through the channel. In the present analysis, *Shirase*'s regular operational speed of 137 rpm was used for all but two cases. The rudder angle is controlled to follow the channel shape and then strongly turned in the direction of turning so that the ship collides with the side of the previous ramming print, which has a curvilinear triangular shape.

**C) Penetration**

After colliding with the ice edge, the ship penetrates the ice under high engine power. The rudder is kept neutral or at a small angle to reduce water resistance. This phase is defined as ended when the ship is at a complete stop for 5 s.

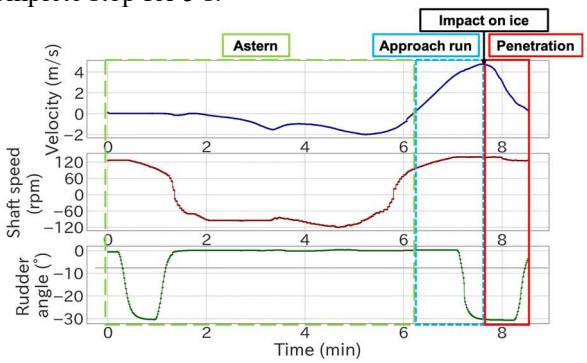


Fig. 1 Typical change of velocity, engine power, and rudder angle during ramming

First, we define the impact velocity ($V$). Because the exact time at which the ship impacts ice is difficult to identify, in this study, we assume that the velocity is maximized when the ship impacts ice. Thus, the impact velocity is defined as the maximum speed during each ramming procedure. Vance (1980) noted that the impact velocity increases with the approach run length ($L$) although it reaches a specific impact velocity with a sufficient approach run length. Through field experiments with the *USCGC Katmai Bay* icebreaker, Vance (1980) also suggested that the impact velocity converged to its maximum after accelerating for 2.5–3.0 ship lengths. For *Shirase*, the impact velocity is controlled at <5–6 m/s to maintain sufficiently low ice pressure on the ship hull. The approach run length needed to achieve this impact velocity is 300–400 m, that is, 2.5–3.0 ship lengths.

Second, we define the penetration distance ($D$) as the distance between the impact point and the ship stopping point. This variable is often used to indicate ramming progress on site. The penetration distance varies with the ice condition and impact velocity.

The turning angle ($\Theta$) is defined as the difference in heading between the first and the last ramming procedure during a turn. It represents the total displacement angle of the turn; it varies between cases because the selected turns do not necessarily reach 180°. $N$ denotes the required number of ramming procedures, and the turning angle per ramming procedure ($\theta$) is calculated as $\Theta/N$.

**2) Projection of ramming positions to *X*–*Y* plane**

The GPS position of the ship stopping point for each ramming procedure is extracted from the above ramming datasets and projected to the *X*–*Y* plane. The longitude and latitude are taken as the *X*- and *Y*-axis directions, respectively, with north and east being positive.

**3) Calculation of turning circle and its radius**

The turning circle is approximated by nonlinear least-squares fitting as the trajectory of each turn. Its radius is calculated and defined as the turning radius ($r$). Although the trajectory of a continuous icebreaking turn is rarely a geometrical circle, we assume it to be a geometrical circle for ramming turns.

## 3. Results and discussion

### *3.1 Turning features*

Table 3 shows the statistics of each turn. The ramming positions and fitted circles are plotted concentrically in Fig. 2. The subscript *av* denotes the averaged values for the turn.

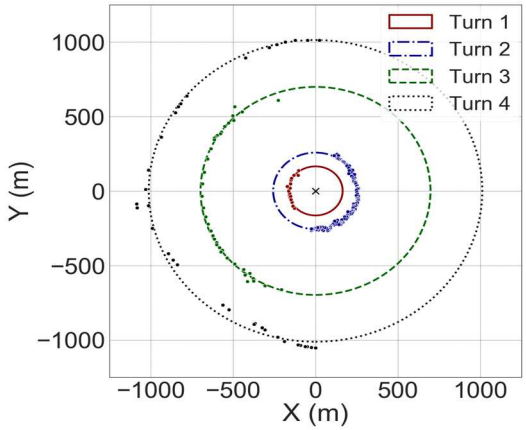


Fig. 2 Concentric plot of ramming endpoints and fitted circles for four turns

Table 3. Statistics of four ramming turns

| | $N$ | $r$ (m) | $V_{av}$ (m/s) | $D_{av}$ (m) | $L_{av}$ (m) | Θ (deg) | $\theta$ (deg) | $h$ (m) |
|---|---|---|---|---|---|---|---|---|
| Turn 1 | 15 | 164.7 | 7.3 | 104 | 264 | 52 | 3.4 | 2.6 / 4.0 |
| Turn 2 | 143 | 257.2 | 6.6 | 52 | 158 | 158 | 1.1 | 4.2 / 4.4 / 5.2 |
| Turn 3 | 39 | 697.9 | 9.0 | 118 | 292 | 142 | 3.6 | 1.7 / 2.1 |
| Turn 4 | 35 | 1012.3 | 6.6 | 143 | 201 | 179 | 5.1 | 2.1 / 2.2 |

Table 4 Maneuverability test results with continuous icebreaking (analyzed by the University of Tokyo, not published)

| | Season | Estimated radius (m) | Ice / snow thickness (m) | Velocity (m/s) | Engine power (rpm) | Rudder angle (deg) |
|---|---|---|---|---|---|---|
| Exp. 1 | December, 2009 | 560 | 0.7~1.0 / 0.3 | 4~4.5 | 137 | 30 (partially 15) |
| Exp. 2 | February, 2010 | 760 | 0.3~0.5 / 0 | 2~4 | 95 | 30 |

The turning radii clearly vary. For two experiments conducted in 2009/2010, the turning radii during continuous icebreaking were 560 and 760 m, respectively (Table 4). The present study shows that the turning radius during ramming sometimes becomes smaller than that during continuous icebreaking.

Fig. 3 shows the quantitative relation between $D$ and $r$. The turning radius increases with the penetration distance. The figure shows the regression formula and its correlation coefficient $R$. Despite the low number of samples, it is expected that the turning radius for an area can be roughly estimated by conducting several ramming procedures and calculating their penetration distances.

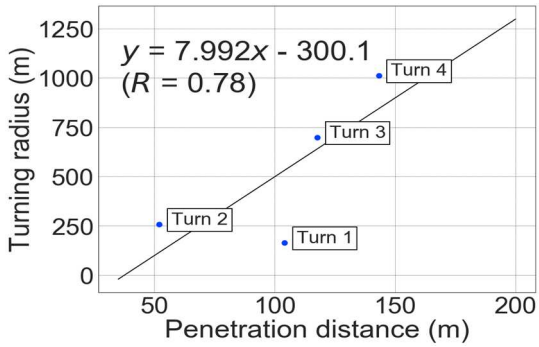


Fig. 3 Relation between penetration distance ($D$) and turning radius ($r$)

Because thicker ice reduces the penetration distance, the turning radius decreases with increasing ice thickness. However, Nozawa (2006) noted that the turning radius with continuous icebreaking increases as a function of ice thickness. The results of the present study are not consistent with this previous report. Here, we discuss the reason for this inconsistency by focusing on the unique features of ramming.

All ramming tracks of Turns 2 and 3 are plotted in Fig. 4 in different colors. The GPS data during penetration only are plotted. This shows that each ramming track is a nearly straight line throughout the turn. In particular, 20 and 10 consecutive ramming examples are extracted from Turns 2 and 3, respectively, and plotted in Fig. 5. This shows that during penetration, the tracks are like straight lines with slight changes in heading angle, although slightly curved tracks are seen in Turn 3.

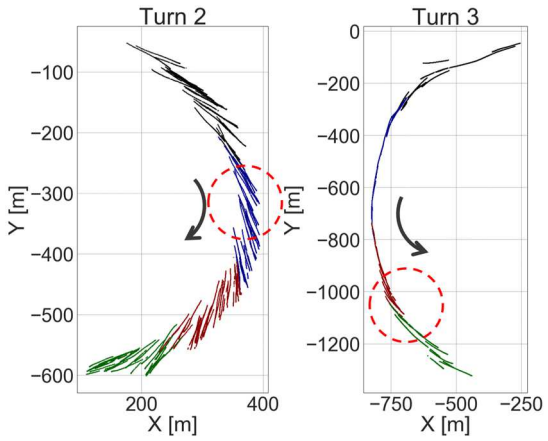


Fig. 4 Tracks during penetration. Red dashed-line circles denote extracted areas shown in Fig. 5.

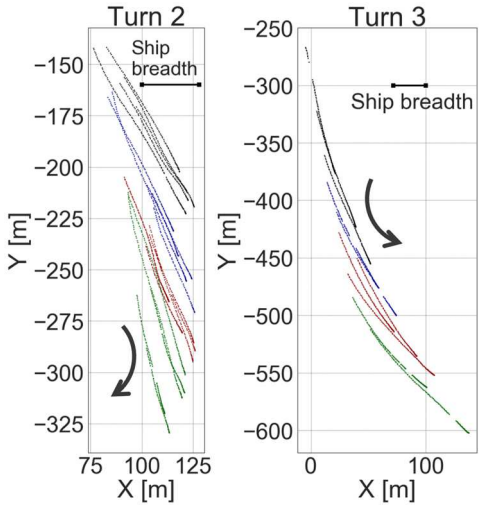


Fig. 5 Tracks during penetration (20 and 10 consecutive ramming procedures from Fig. 4 extracted for magnification.)

The relationship shown in Fig. 3 can be explained as follows. The turning angle is mainly achieved during the approach run and less so, if at all, during penetration. Therefore, longer penetration distances expand the tracks outward, thereby lengthening the turning radius compared to that in gradual (short penetration distance) ramming.

If this holds under all conditions, it is possible that the longer penetration distance does not contribute to the efficiency of a ramming turn. In fact, gradual ramming with shorter penetration distances may be more efficient because of the shorter trajectory. It is critical to determine whether the turning angle is achieved to any extent during penetration.

To discuss this more quantitatively, the time series data of the ship's yaw rate and velocity are shown in Fig. 6. Each line represents each turn, as obtained by averaging each ramming procedure after aligning the procedures such that the impact timing on the ice is 0 s. The turning direction is considered positive for the yaw rate plot of each turn. The yaw rate is clearly maximized during the approach run, and it decreases rapidly after impact. This is attributed to the ship bouncing from the ice edge. The yaw rates of Turns 3 and 4, which have long penetration distances, remain positive for a while. Although the yaw rate does not necessarily coincide with the angle of the navigation track, it implies that some of the turning angle can be achieved during the penetration phase. However, the amount is smaller than that during acceleration, such that the turning radius is increased, as in the discussion following Fig. 5.

For greater clarity, the turning angle per ramming procedure θ is calculated for each turn by dividing the total change in angle by the number of ramming procedures. The result is shown in Fig. 7, with the penetration distance plotted on the horizontal axis.

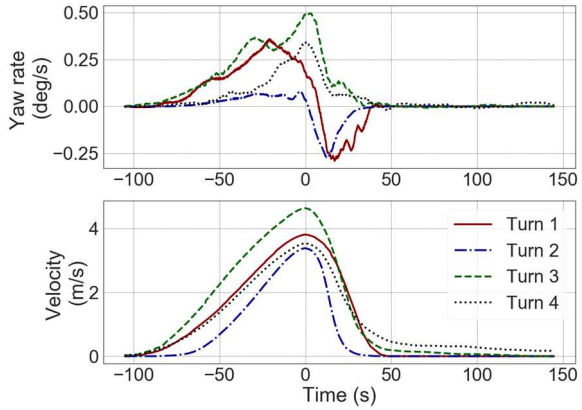


Fig. 6 Averaged yaw rate change and velocity change during ramming for each turn

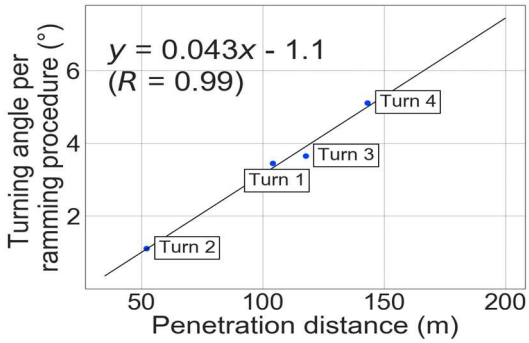


Fig. 7 Relation between penetration distance (D) and turning radius per ramming procedure (θ)

The result shows a clear positive near-linear correlation between the penetration distance and the turning angle per ramming procedure. It can be expected that the required number of ramming procedures to achieve a certain change in angle can be estimated from the penetration distances of several ramming trials, thus yielding the total time required for turning. Because the penetration distance can be observed and calculated easily on site and in real time, this is considered useful for navigation planning.

### *3.2 Discussions on efficient turning*

Next, we attempted to improve the efficiency of the turning operation based on the above results. The conceptual diagram is shown in Fig. 8.

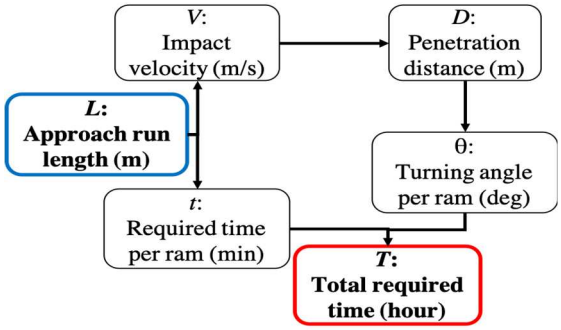


Fig. 8 Conceptual diagram of calculation

The approach run length ($L$) is chosen as the predictor variable. The navigation officer can control this easily by changing the timing to stop the astern movement. The total required time ($T$) is defined as the total time required for turning by a certain angle, which is the objective variable to reduce. When we consider a turn of $\Theta$, $T$ can be decomposed into the following equations:

$$T = (\Theta/\theta) \cdot t \quad (1)$$
$$\theta = a_\theta \cdot D + b_\theta \quad (2)$$
$$D = a_D \cdot V + b_D \quad (3)$$
$$V = a_V \cdot L + b_V \quad (4)$$
$$t = a_t \cdot L + b_t \quad (5)$$

Therefore, $T$ can be expressed as an equation of only one variable $L$:

$$T = \frac{\Theta \cdot (a_t \cdot L + b_t)}{a_\theta \cdot (a_D \cdot (a_V \cdot L + b_V) + b_D) + b_\theta} \quad (6)$$

Here, $a$ and $b$ with subscripts denote constants, and $t$ is the time required per ramming procedure during the turn. Tatinclaux (1992) noted that the penetration distance $D$ is a linear function of the impact velocity $V$, although the relational expression varies for different ice conditions. The coefficients of the relational expression are calculated for the four areas of turning, as shown in Fig. 9. At this time, it is difficult to identify a tendency between the ice conditions and the features of the regression lines.

We assumed that the dependency of $\theta$ on $V$ can be calculated from the relations shown in Fig. 7 and Fig. 9. Though the above discussion indicates that changes in $V$ affect $D$ and thus $\theta$, it is also possible that this effect is small and that the relation shown in Fig. 7 is largely due to the effects of ice condition differences on both $D$ and $\theta$ separately. For an accurate calculation, the contribution of $V$ to $\theta$ should be quantified without ice condition differences. Because of the shortage of data for such quantification, we assumed that the regression formula shown in Fig. 7 is applicable to the change in $D$ accompanying the change in $V$. Considering this uncertainty, we calculated seven scenarios: relational expression of the original regression line, 20% raised/inclined, 10% (of average of four turns) parallel upward/downward shifted, and 20% increased/decreased uniformly (Fig. 12).

$V$ and $t$ change depending on $L$. The relation among $V$, $t$, and $L$ is calculated in the same manner as above. Preceding icebreaking tests of *Shirase* (2010/2011, result not published) suggested that the relation between $L$ and $V$ was linear and that the relational expression did not vary significantly for different ice conditions. This is justified because the icebreaker passes an open water channel during the approach run. The results of the present analysis agree with this report, as shown in Fig. 10. However, the correlation between $L$ and $t$ varies for the four turns (Fig. 11). This is attributed to effects on the relation by brash ice coverage in the channel generated by the icebreaker itself. The quantity of produced brash ice is greater in thicker ice areas (i.e., Turns 1 and 2). If the brash ice in the channel is increased, the ice resistance is increased, and thus, the required time per unit length astern distance is longer. Therefore, it is reasonable that the regression lines of Turns 1 and 2 (thicker ice areas) are steeper than those of Turns 3 and 4 (thinner ice areas).

In the regression analyses, some irregular ramming procedures are removed:

1) Extreme penetration distances despite low impact velocities

Two ramming procedures with penetration distances >200 m are removed from Turn 3. Such ramming procedures can be caused by partially thin ice, though the actual cause has not been identified.

2) Low engine power

Two ramming procedures are performed at low velocity because low engine power is used.

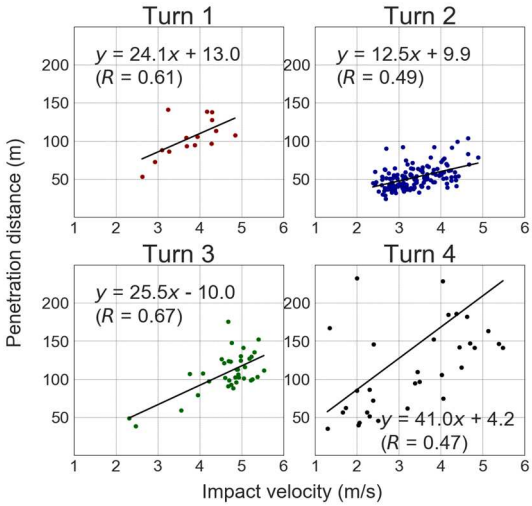


Fig. 9 Regression analysis between impact velocity ($V$) and penetration distance ($D$)

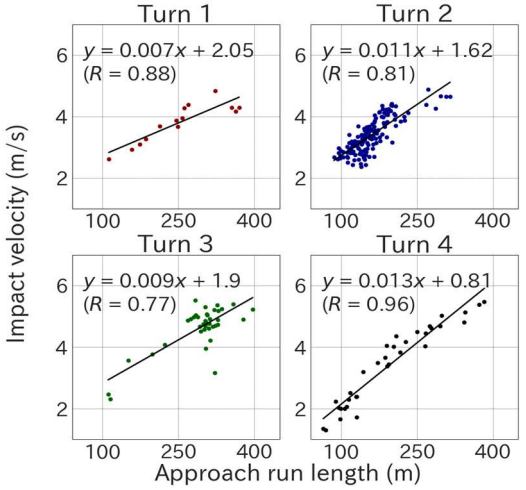


Fig. 10 Regression analysis between approach run length ($L$) and impact velocity ($V$)

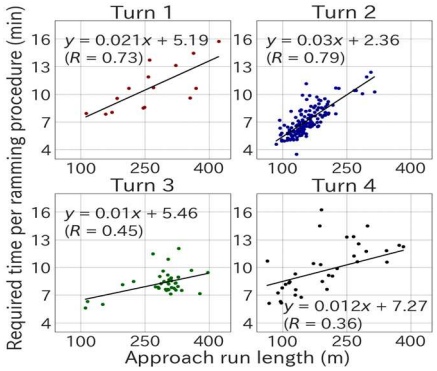


Fig. 11 Regression analysis between approach run length ($L$) and required time per ramming procedure ($t$)

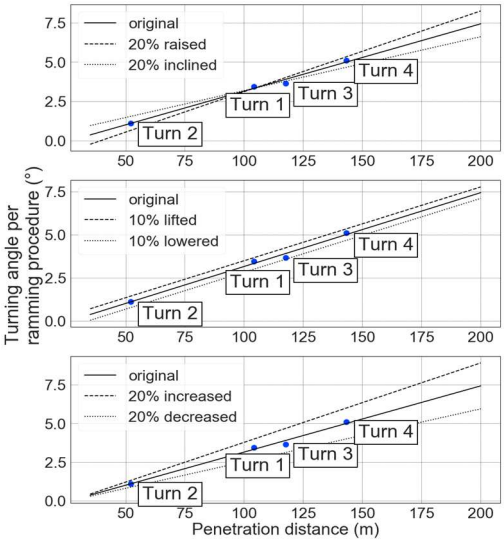


Fig. 12 Relational expressions of seven scenarios between penetration distance ($D$) and turning angle per ramming procedure ($\theta$)

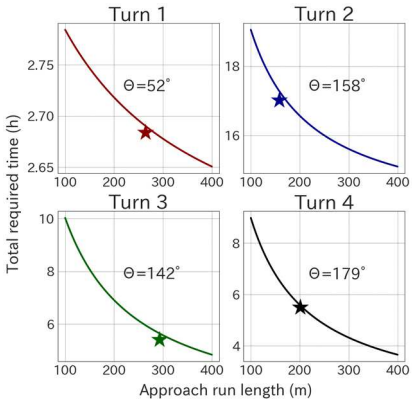


Fig. 13 Estimated total required time ($T$) and its dependency on approach run length ($L$). Actual time–length point for each turn is indicated by a star.

By using the relational expressions mentioned above, $T$ is calculated for various $L$ values in the feasible range of 100–400 m. The results are shown in Fig. 13 and Fig. 14. These estimations are compared to the actual required times and averaged approach run lengths.

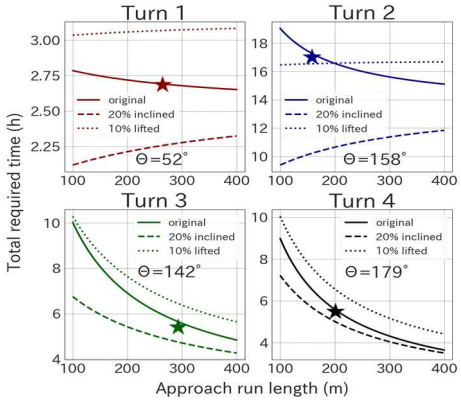


Fig. 14 Estimated total required time ($T$) and its dependency on approach run length ($L$) – scenarios of 20% inclined/10% lifted (parallel upward shift) from the original $D$–$\theta$ equation. Actual $L$–$T$ values are indicated using stars.

In the scenario with the original $D$–$\theta$ regression lines (Fig. 13), $T$ decreases monotonically with $L$ for all four cases. The actual data lies almost on the lines, indicating the reliability of the calculation scheme. The result implies that the approach run length should be increased for a time-efficient turn.

However, Fig. 14 shows that the $L$–$T$ correlations for Turns 1 and 2 change from negative to positive in two scenarios whereas for Turns 3 and 4, they are negative for all three scenarios. The scenarios not plotted in this figure are all decreasing functions. The reason for this is explained below.

The conditional expression for $T$ as a decreasing function of $L$ is

$$\frac{dT}{dL} \leq 0 \qquad (7.1)$$

By calculating this using equation (6), we obtain:

$$-a_D\, a_V\, a_\theta\, b_t + a_t\, b_\theta + a_D\, a_t\, a_\theta\, b_V + a_t\, a_\theta\, b_D \leq 0 \qquad (7.2)$$

Here, we conducted a sensitivity study as follows:

1) The average and standard deviation of each coefficient were calculated for the four turns. For $a_\theta$ and $b_\theta$, the value itself is used for the mean value and 50% of its value is substituted for the standard deviation as a guide.
2) The standard value is calculated by substituting the averaged coefficients into the left-hand side of (7.2).
3) Each coefficient is increased by its standard deviation while holding the others constant, and the difference from the standard value is calculated for each coefficient (hereafter defined as sensitivity).

The results are shown in Table 5. It shows that $b_t$ has the greatest influence compared to the other coefficients. This suggests that the $L$–$t$ relation has the greatest contribution to the shape of the $L$–$T$ curve. Here, we must consider that $b_t$ changes depending on

$a_t$ in the process of regression analysis. This complication arises because the linear model assumption is not applicable for small values of $L$ (< 100). Theoretically, $t$ at $L$ = 0 should be constant regardless of ice conditions.

Based on the above discussion, the results shown in Fig. 14 can be explained as follows. In Turns 1 and 2, heavy ice conditions yield regression lines with larger $a_t$ and smaller $b_t$ (see discussion on page 17), thus making *dT/dL* positive.

Table 5 Sensitivity of *dT/dL* to each coefficient

| $a_t$ | $b_t$ | $a_V$ | $b_V$ | $a_D$ | $b_D$ | $a_\theta$ | $b_\theta$ |
|---|---|---|---|---|---|---|---|
| 0.01 | -11.36 | 0.00 | -0.28 | -0.13 | 0.21 | 0.00 | -0.02 |

These results suggest that the approach run length should be lengthened for time-efficient turns, especially when brash ice coverage in the channel is low and the approach run length can be increased relatively freely. However, this does not always apply if brash ice fills the channel.

For predicting the total required time, Fig. 13 and Fig. 14 show that the total time changes by up to 50% depending on the approach run length. Again, if the brash ice prevents a long approach run, the turn may require more time than that predicted using the relation shown in Fig. 7. Further studies are required for the practical prediction of the total required time for turning while ramming.

## 4. Conclusions

The turning performance under ramming operation is investigated by analyzing data from four turns conducted in actual ice-covered sea. As a result, the following features of ramming turns are obtained:

- The turning radius increases almost linearly with penetration distance.
- The turning angle per ramming procedure increases with the penetration distance despite the longer trajectory.
- The total required time for turning decreases with increasing approach run length for 100–400 m runs, unless brash ice significantly prevents the ship's astern movement.

Based on these results, the following navigation guidelines for ramming turns are suggested:

- To reduce the turning time, the approach run length should be increased unless brash ice significantly fills the channel.
- For an icebreaker that is forced to turn in a narrow area, it may be effective to shorten the penetration distance to achieve small turns.
- It is expected that the total required time for turning can be estimated using the penetration distances of the first several ramming procedures during a turn, although this method has low reliability based on the results of the present study.

To confirm the validity of the analysis, a field experiment of two turns in one area with varying approach run lengths is desired. In addition, turns performed by other icebreakers must be investigated to generalize the results. It has already been suggested that the turning performance during continuous icebreaking varies depending on the shape of the ship (Nozawa, 2006; Sazonov, 2011).

## Acknowledgements

The authors wish to acknowledge support from Japanese Antarctic Research Expeditions (JAREs) and a "Kaken-hi" grant (no. 26249133) from the Japan Society for the Promotion of Science. We also thank the ship crew of JARE 59 for their cooperation. We are also indebted to the Antarctic Research Support Section, Ministry of Defense, for their permission to publish this work. We thank Dr. Ito (Institute of Low Temperature Science, Hokkaido University) for providing ice observation data.

## References

Daley, C. G. and K. Riska (1990): *Review of Ship-ice Interaction Mechanics Report from Finnish-Canadian Joint Research Project No.5 "Ship Interaction With1 Actual Ice Conditions" Interim Report on Task 1A*. Helsinki, Finland: Helsinki University of Technology

Nozawa, K. (2006): *Engineering for ice-covered seas*. Tokyo, Japan: Seizando-Shoten Publishing Co., Ltd. (in Japanese)

Sazonov, K. E. (2011): Navigation challenges for large-size ships in ice conditions. *Ship and Offshore Structures*. **6:3**. 231-238. doi: 10.1080/17445302.2010.548123

Shimoda, H., T. Endoh and 6 others (1997): Observation of sea-ice conditions in the Antarctic coastal region using ship-board video cameras. *Nankyoku-Shiryo (Antarctic Record)*. **41(1)**. 355-365. (in Japanese)

Tatinclaux, J. C. (1992): Tests in ice on an Antarctic research vessel model. Retrieved from http://www.dtic.mil/ dtic/tr/ fulltext/u2/a249789.pdf

Vance, G. P. (1980): Analysis of the performance of a 140-foot Great Lakes icebreaker USCGC KATMAI BAY (No. CRREL-80-8). *Cold Regions Research and Engineering lab Hanover NH*.

Yamauchi, Y. and S. Mizuno (2009): Study on improvement in ramming performance of Antarctic icebreaker. *Proc. of the 19th International Offshore and Polar Engineering Conference (ISOPE-2009)* CD-ROM. 629-635.

Yamauchi, Y., S. Mizuno and H. Tsukuda (2011): The icebreaking performance of SHIRASE in the maiden Antarctic voyage. *Proceedings of the 21th International Offshore and Polar Engineering Conference (ISOPE-2011)* CD-ROM. 1093-1099.